Supplementary material

Graphitic C₃N₄ nanocomposite-based fluorescence platform for label-free analysis of trace mercury ions

Xinrong Guo[a], Wen Yao[a], Silan Bai[b], Junhui Xiao[b], Yubo Wei[c*], Lishi Wang[b*], Jie Yang[a*]

_____

a: Dongguan Key Laboratory of Public Health Laboratory Science, School of Public Health, Guangdong Medical University, Dongguan 523808, People's Republic of China

b: School of Chemistry and Chemical Engineering, South China University of Technology, Guangzhou 510641, People's Republic of China. Tel: +86 020 87112906.

c: School of Pharmaceutical Sciences and Yunnan Key Laboratory of Pharmacology for Natural Products, College of Modern biomedical industry, Kunming Medical University, People's Republic of China

E-mail address: weiyubu@kmmu.edu.cn

E-mail address: wanglsh@scut.edu.cn

E-mail address: Yang_J@gdmu.edu.cn

Table of Contents:

1. Experimental section

1.1 Reagent

Urea and citric acid were purchased from Agilent Technologies Co., Ltd. (Beijing, China). Chemicals such as sodium hydroxide (NaOH), sodium chloride (NaCl), mercuric chloride ($FeCl_3$), phosphoric acid (H_3PO_4, 85%), acetic acid (CH_3COOH), boric acid (H_3BO_3), nitric acid (HNO_3), mercury ions (Hg^{2+}) and other interfering substances were purchased from Fuchen Chemical Reagent Factory (Tianjin, China). All the chemicals used throughout the experiment were of analytical grade and had not undergone any treatment prior to use. The solution involved in the experiment were all prepared using ultrapure water with a resistance of 18.2 MΩ·cm.

1.2 Instruments

The JEOL-2010F transmission electron microscope (TEM, Hitachi, Japan) was used to investigate the morphology of the CNQDs/CNNNs composite materials. The VERTEX 70 Fourier-transform infrared spectrometer (FT-IR, Bruker, Germany), UV-3010H Ultraviolet-Visible diffuse reflection spectra (DRS, Hitachi, Japan), ESCALAB 250Xi X-ray photoelectron spectrometer (XPS, Thermo Scientific, USA), and D4 X-ray diffractometer (XRD, Bruker, Germany) were used to study the chemical structure, bandgap, chemical valence states, and crystal structure of the CNQDs/CNNNs, respectively. The FluoroMax-4 fluorescence spectrophotometer (HORIBA, USA) was used to observe the changes in emission peak fluorescence intensity of the CNQDs/CNNNs without and with Hg^{2+}. The UV-3900H spectrophotometer (Hitachi, Japan) was used to study the interaction between CNQDs/CNNNs and Hg^{2+}. The SZ-100 nanometer particle size and zeta potential analyzer (Bruker, Germany) were mainly used to investigate the zeta potential and dynamic light scattering of the CNQDs/CNNNs. The ZF-2 ultraviolet lamp (Hangzhou Qiwei Instrument & Electronics Co., Ltd., China) was used to observe fluorescent changes in the solution throughout the experimental process.

1.3 Synthesis of CNQDs/CNNNs

In this study, a simple and efficient one-step pyrolysis process was used to synthesize CNQDs/CNNNs based on previous report with slight modifications[1,2]. briefly, a mixture of 0.1009 g urea and 0.0588 g citric acid was ground for 30 min, and then transferred to a porcelain crucible and reacted at 180°C for 1 h. After natural cooling to room temperature, a light-yellow solid was obtained and dissolved in a mixed solution of ethanol and distilled water, washed, filtered, and dried under vacuum at 60°C to obtain the solid product. The solid was then dissolved in distilled water to obtain CNQDs/CNNNs solution, which was stored at 4°C for later use.

1.4 Construction fluorescence sensing platform of the CNQDs/CNNNs for Hg^{2+} detection

The CNQDs/CNNNs-based fluorescence sensor was used to quantify Hg^{2+}. Firstly, adding 50 μL 1.0 mg mL^{-1} of the CNQDs/CNNNs solution to a 0.1 mol L^{-1} B-R buffer solution (pH=7.0). Secondly, adding 50 μL of Hg^{2+} with different concentrations to the mixed solution (a total of 23 concentrations, ranging from 0 to 175.5 μmol L^{-1}). Finally, the solution was diluted to 2.0 mL with distilled water. After thoroughly mixing the solution at room temperature, monitoring the fluorescence spectrum in the wavelength range of 380-700 nm.

1.5 DFT simulations mechanism

In this work, one of the layered g-C_3N_4 (CN) was selected as the calculation model of synthesized CNQDs/CNNNs. All spin-polarized density functional theory calculations were performed using the Vienna ab initio simulation package (VASP). The interactions of Hg^{2+} with CNQDs/CNNNs were investigated by the D3 correction approach (DFT-D3). The Perdew-Burke-Ernzerhof (PBE) functional's generalized gradient approximation (GGA) was used to handle the exchange-functional. The projector-augmented wave (PAW) method was utilized to indicate core-valence interactions. Gaussian smearing with a smearing width of 0.05 eV was employed for electron smearing. The plane wave basis expansion energy cutoff was set at 500 eV. The conjugate gradient algorithm was used to minimize the forces on each

ion until they were below 0.02 eV/Å to obtain optimized structures. Convergence energy threshold of 10^{-5} eV was used for self-consistent calculations. The Monkhorst-Pack K-mesh, with a K-point separation of 0.04 $Å^{-1}$, was applied for Brillouin-zone integration.
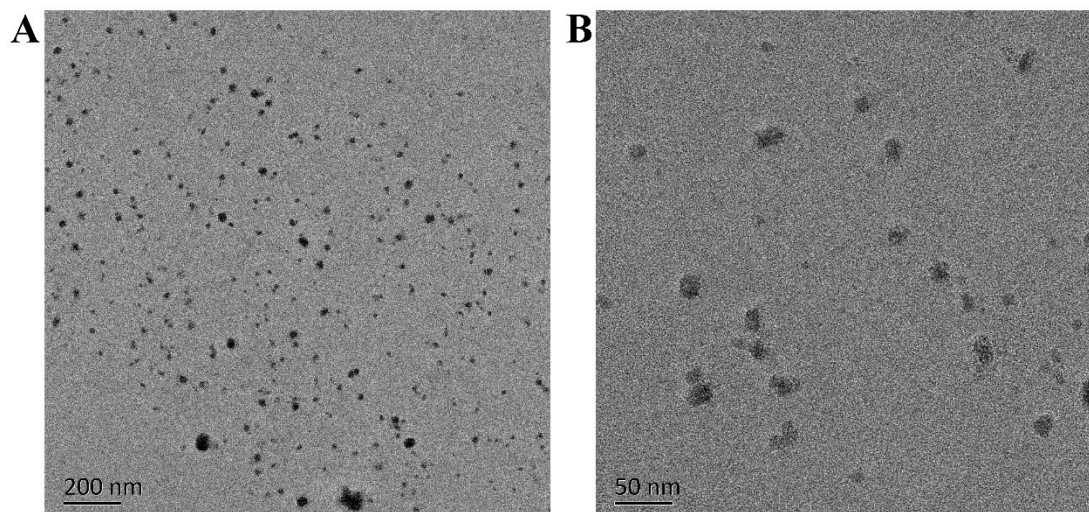
2. The TEM characteristics of the CNQDs/CNNNs

Figure S1 The low (A) and high magnification (B) TEM images of the CNQDs/CNNNs.

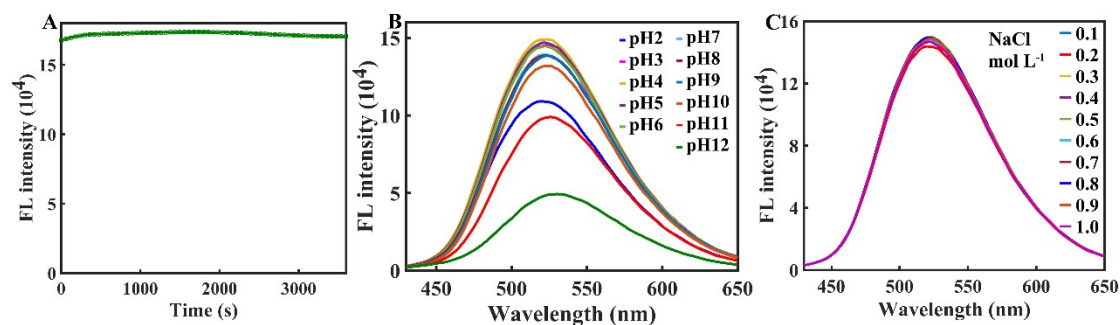## 3. Optical characteristics of the CNQDs/CNNNs

Figure S2 (A) Effect of 150 W xenon lamp irradiation for one hour on the fluorescence intensity of the CNQDs/CNNNs; (B) Fluorescence spectra of the CNQDs/CNNNs under different media pH conditions; (C) Fluorescence spectra of the CNQDs/CNNNs under different salt concentration conditions.

4. Optimization of experimental condition

To enhance the performance of the CNQDs/CNNNs-based fluorescence sensor for the detection of Hg^{2+}, various experimental conditions were optimized, including the reaction time and the pH of medium. To investigate the reaction, a B-R buffer solution (pH=7.0) was employed, CNQDs/CNNNs and 20 μmol L^{-1} Hg^{2+} were sequentially added, and the fluorescence intensity was recorded at 520 nm immediately following thorough mixing. The observed results revealed that the fluorescence intensity of CNQDs/CNNNs drastically decreased upon addition of Hg^{2+}, indicating that the reaction is a rapid quenching process (Figure S3A). Further investigated the effect of pH on the quenching effect of Hg^{2+} on the CNQDs/CNNNs fluorescence. The B-R buffer solution with a pH ranging from 2.0 to 12.0 was used as the reaction medium. In highly acidic (pH=2) or highly alkaline (pH=11-12) media, the fluorescence intensity of CNQDs/CNNNs decreased considerably without the addition of Hg^{2+}. However, the influence of pH on the fluorescence intensity was insignificant when the pH ranged from 3 to 10. After addition of Hg^{2+}, the fluorescence intensity of CNQDs/CNNNs considerably decreased, and the difference value between without and with Hg^{2+} was the greatest when the pH was 7.0. Thus, the optimal pH is 7.0 (Figure S3B).
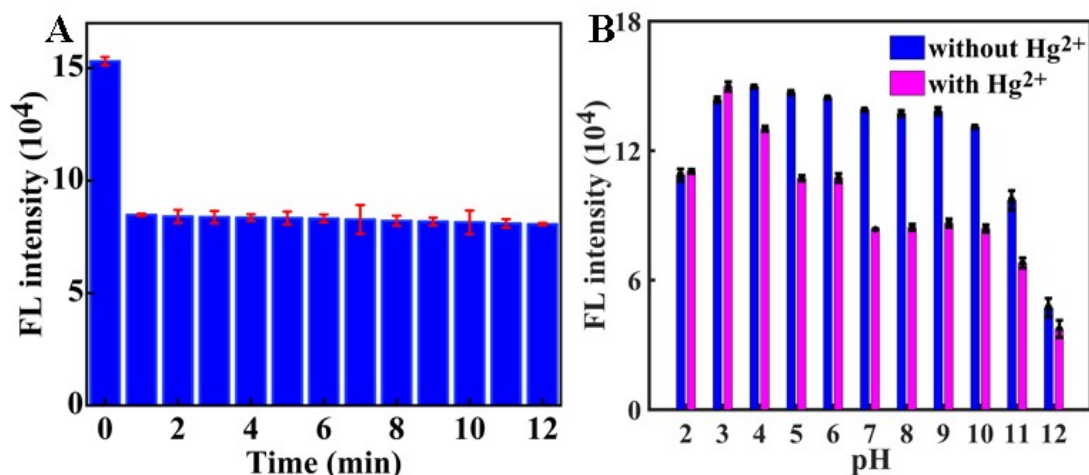

Figure S3 (A) Effect of fluorescent intensity for the CNQDs/CNNNs without and with Hg^{2+} in different reaction times; (B) Effect of fluorescent intensity for the CNQDs/CNNNs without and with Hg^{2+} in different pHs.

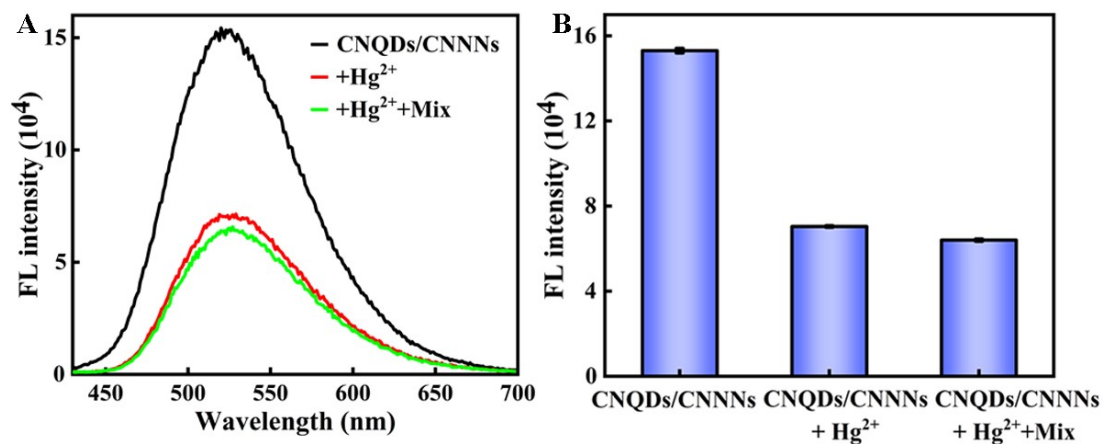## 5. The selectivity test of the CNQDs/CNNNs with Hg^{2+}

Figure S4 (A) The fluorescence spectra of the CNQDs/CNNNs without and with Hg2+ in the absence and presence of mix ions. (B) The effects of the afore-mentioned metal ions on the fluorescence of the CNQDs/CNNNs.
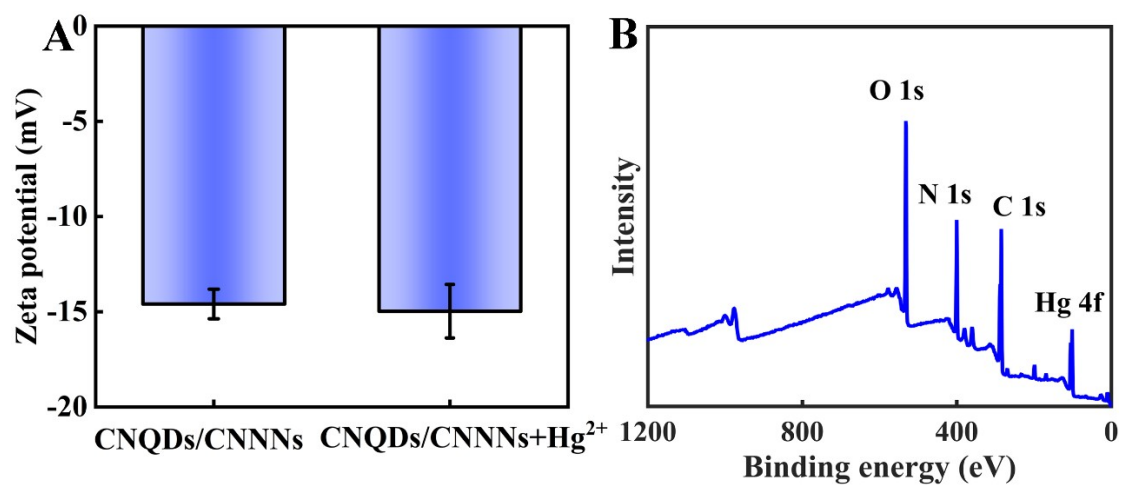
6. The XPS spectrum of the CNQDs/CNNNs with Hg^{2+}

Figure S5 (A) The Zeta potential of the CNQDs/CNNNs without and with Hg^{2+}. (B) The survey spectra of CNQDs/CNNNs in the precent of Hg^{2+}.

7. **The side view of geometric structure of the CN without or with Hg²⁺**
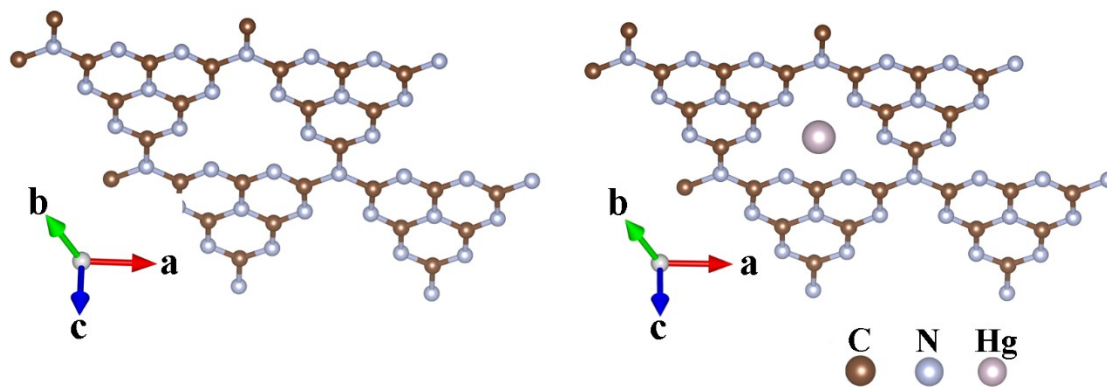

Figure S6 The side view of geometric structure for the CN sheet and CN-Hg.

8. **The study of change density for the CN without or with Hg²⁺**
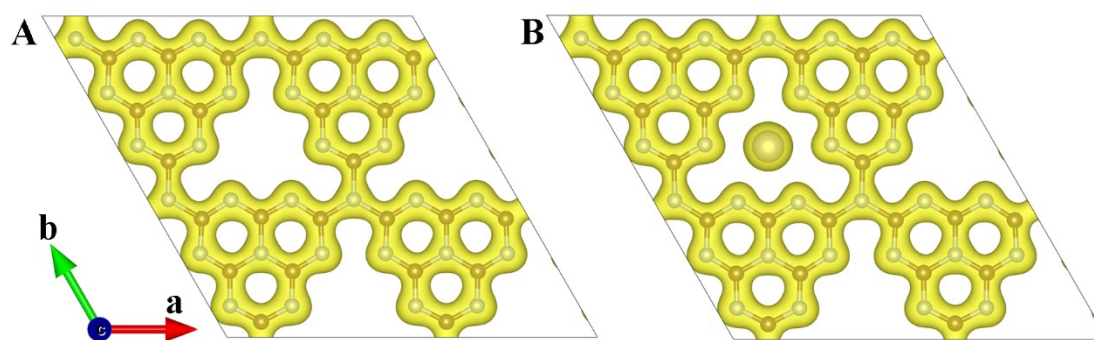

Figure S7 The change density of CN (A) and CN-Hg (B).

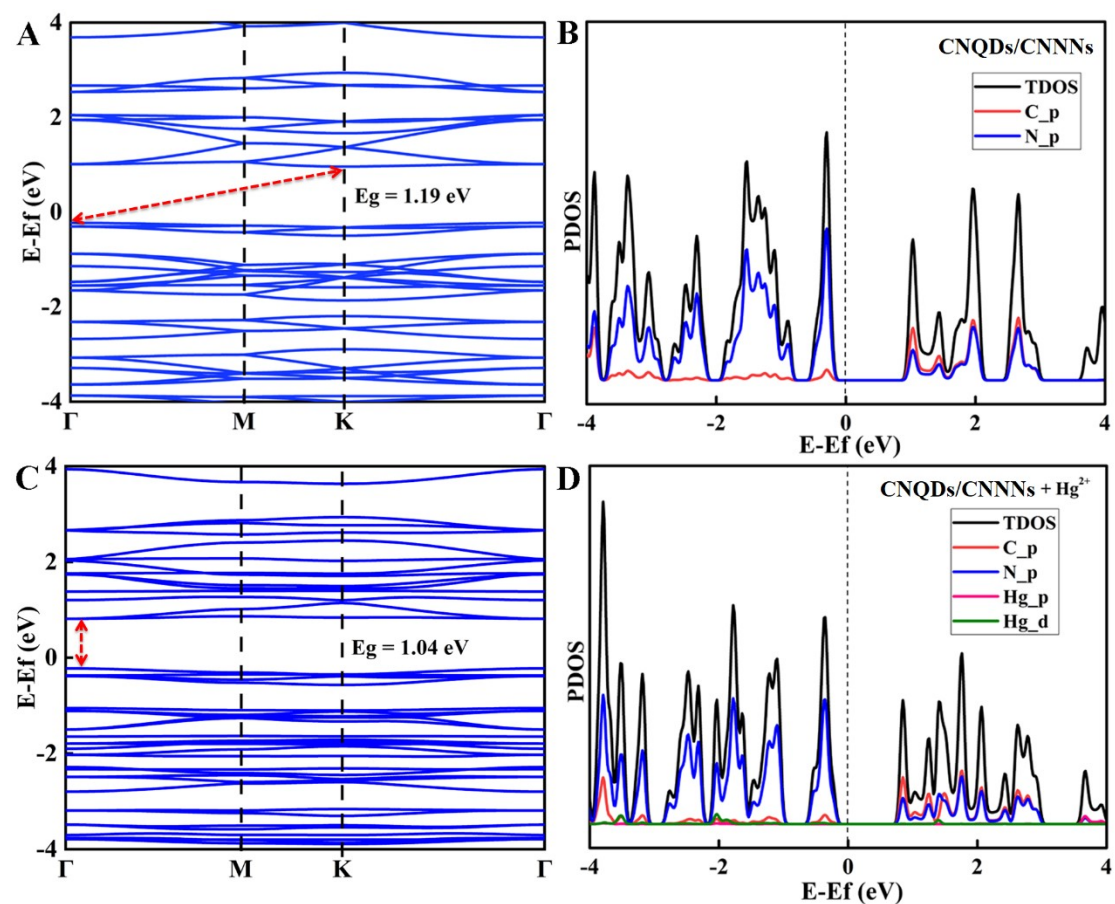## 9. The bag energy and POSD for the CN without or with Hg²⁺

Figure S8 The band structure (A) and PDOS (B) for the CN layer. The band structure (C) and PDOS (D) for the CN layer after interacting with Hg.

10. The CNQDs/CNNNs-based fluorescent sensor compared with other reported fluorescence sensors for analysis of Hg^{2+}

Table S1 The CNQDs/CNNNs-based fluorescent sensor compared with other reported fluorescence sensors for analysis of Hg^{2+}

Probes	Mechanism	Linear range （$\mu mol\ L^{-1}$）	LOD (nmol L^{-1})	Ref.
CDs/InPQDs@ZIF-8[a]	Electron transfer	0-0.500	8.68	3
CDs	Hg-S bond	0.09-16.2	447	4
CDs-AgNPs[b]	higher affinity	100-160	22.2	5
Fe-MIL-88NH$_2$/AuNCs[c]	Electron transfer	0.002-30	7.00	6
MSN@Py-EOA[d]	coordinate complex	1-20.0	620	7
T/G-C$_3$N$_4$ NNs[e]	Electron transfer	0-1.25	27.0	8
g-C$_3$N$_4$ QDs	Static quenching	0.2-21.0	3.30	9
g-C$_3$N$_4$ NNs	Electron transfer	2.5-25.0	37.0	10
CNQDs/CNNNs	Interaction	0.025-4.00	7.82	This work

[a]: Blue fluorescent carbon dots (CDs), red fluorescent InP/ZnS quantum dots (InPQDs), and MOFs (ZIF-8) integrated multicolor nano-sensor (CDs/InPQDs@ZIF-8)

[b]: Carbon dots (CDs) and silver nanoparticles (CDs-AgNPs)

[c]: the fluorescence sensing platform system of the ironbased metalorganic framework (Fe-MIL-88NH$_2$) and gold nanoclusters (Au NCs) (Fe-MIL-88NH$_2$/AuNCs)

[d]: immobilizing the pyrene derivative on epoxy-terminated mesoporous silica nanoparticles (MSN@Py-EOA)

[e]: The functionalized graphitic carbon nitride nanosheets (T/G-C$_3$N$_4$) fluorescence probe was fabricated using melamine as a precursor by the pyrolysis technique, followed by a rapid KOH heat treatment method for 2 min.

11. Construction of CNQDs/CNNNs sensor for Hg^{2+} detection in natural sample

Table S2 Quantitative detection of Hg^{2+} in lake water samples by spiking method for the CNQDs/CNNNs fluorescent sensors （n=3）

Samples[a]	Detected	Added (μM)	Found（μM）	Recovery (%)	RSD (%)
1[#]	ND [b]	0.04	0.039	97.5	1.2
2[#]	ND	0.4	0.405	101.2	4.5
3[#]	ND	4.0	4.01	100.2	2.7

[a] Water samples were collected from the lake in the north campus for South China University of Technology, which were spiked with different concentrations of Hg^{2+}

[b] Not detection of Hg^{2+}

Reference

1   M. Shorie, H. Kaur, G. Chadha, K. Singh, P. Sabherwal, *Journal of Hazardous Materials*, 2019, **367,** 629-638.

2   P. Liu, Y. Sun, S.F. Wang, H. J. Zhang, Y. N. Gong, F. J. Li, Y. F. Shi, Y. X. Du, X. F. Li, S. S. Guo, Q. D. Tai, C. L. Wang, X. Z. Zhao, *Journal of Power Sources*, 2020, **451,** 227825.

3   L. N. Zhang, Y. R. Xu, J. Xu, H. J. Zhang, T. Q. Zhao, L. Jia, *Journal of Hazardous Materials*, 2022, **430,** 128478.

4   H. Yang, X. K. Su, L. Cai, Z. C. Sun, Y. C. Lin, J. Yu, L. K. Hao, C. Liu, *Journal of Environmental Chemical Engineering*, 2022, **10,** 108718.

5   K. Y. Zhang, Y. X. Sang, Y. D. Gao, Q. X. Sun, W. N. Li, *Spectrochimica Acta Part A-Molecular and Biomolecular Spectroscopy*, 2022, **264,** 120281.

6   Z. W. Lu, J. Li, K. Ruan, M. M. Sun, S. X. Zhang, T. Liu, J. J. Yin, X. X. Wang, H. P. Chen, Y. Y. Wang, P. Zou, Q. M. Huang, J. S. Ye, H. B. Rao, *Chemical Engineering Journal*, 2022, **435,** 134979.

7   Z. J. Wang, Z. P Gao, M. Qiao, J. X. Peng, L. P. Ding, *Colloids and Surfaces A-Physicochemical and Engineering Aspects*, 2022, **637,** 128269.

8   Y. G. A. EI-Reash, E. A. Ghaith, O. EI-Awady, F. K. Algethami, H. Q. Lin, E. A. Abdelrahman, F. S. Awad, *Journal of Analytical Science and Technology*, 2023, **14,** 16.

9   X. Wang, X. F. Yang, N. Wang, J. J. Lv, H. J. Wang, M. M. F. Choi, W. Bian, *Microchimica Acta*, 2018, **185,** 471.

10   J. L. Duan, Y. H. Zhang, Y. B. Yin, H. S. Li, J. Wang, L. S. Zhu, *Sensors and Actuators B-Chemical*, 2018, **257,** 504-510.